PERGAMON

International Journal of Solids and Structures 37 (2000) 1701–1726

INTERNATIONAL JOURNAL OF SOLIDS and STRUCTURES

www.elsevier.com/locate/ijsolstr

Wave reflection from the free end of a cylinder with an arbitrary cross-section

H. Taweel[a], S.B. Dong[a,*], M. Kazic[b]

[a]*Civil and Environmental Engineering Department, University of California, Los Angeles, CA 90095-1593, USA*
[b]*Schwoerer GmbH and Co., Stuttgart, Germany 70182*

Received 26 February 1998; in revised form 27 February 1998

Abstract

Elastic wave scattering at the free end of a cylinder due to an incident monochromatic wave is investigated. The cross-section may have an arbitrary geometry with any number of distinct elastic rectilinear anisotropic materials comprising its planar profile. The governing equations are based on a semi-analytical finite element method in which the cross-sectional behavior is modeled by general two-dimensional finite elements with the axial dependence and time left unspecified at the outset. First, all the modal data for the cylinder are established. Two eigenproblems are posed for this purpose, that are obtained by inserting a wavelike solution form into the governing equations. These eigenproblems allow all propagating waves and end modes for the cylinder to be determined. Propagating modes are traveling waves with energy transport capabilities, while the end modes are standing vibrations which, in contrast, do not transport any energy into the interior of the cylinder. These eigendata are the basis for representing the wave reflection phenomenon at the free end. The amplitudes of the traveling waves and end modes that satisfy traction-free end conditions may be determined by least-squares minimization or by a virtual work method. Four cylinders with different cross-sectional geometries were considered to illustrate the analysis procedure and reveal some physical insight into the frequency dependent wave reflection phenomena in them.

1. Introduction

In this paper, we consider the reflection of a monochromatic wave train impinging upon the free end of a semi-infinitely long prismatic cylinder. The proposed analysis technique can accommodate a cylinder with an arbitrary cross-sectional shape that is made up of different anisotropic materials which are perfectly bonded at all common interfaces. This general problem enjoys a crucial role in non-

* Corresponding author.
E-mail address: dong@seas.ucla.edu (S.B. Dong)

0020-7683/00/$ - see front matter
PII: S0020-7683(98)00301-1

destructive evaluation (NDE) methods, which rely on wave scattering data to locate and estimate the size and/or extent of cracks, voids and other flaws in them. Herein, we restrict our scope to the end reflection problem of undamaged bars, as such a study is a required initial step toward the ultimate goal of supporting NDE methods.

When a traveling monochromatic wave of frequency ω arrives at the free end of a cylinder, its incidence on this surface causes a scattering phenomenon that involves reflected traveling waves as well as a host of end vibrations or end modes. Only the traveling waves have the capability of carrying the incident wave energy back into the interior of the cylinder. However, the incident wave and all possible reflected traveling waves by themselves do not in general satisfy traction-free end conditions. These traveling waves must be supplemented by a series of end modes in order to have a traction-free end. End modes are associated with purely imaginary and/or complex wave numbers k in the axial wave form e^{ikz} where z is the propagation axis, so that their mathematical wave forms show monotonically and damped sinusoidal decay into the interior. These modes also lack the capacity of conducting any energy into the interior of the cylinder.

Historically, the study of vibrations and waves based on three-dimensional elasticity began with Pochhammer (1876) and Chree (1889) who independently gave the governing equations, outlined the solution form and generated the frequency equation for a homogeneous, isotropic circular cylinder. Extraction of roots from this frequency equation laid fallow for more than fifty years before Bancroft (1941), Hudson (1943) and Davies (1948) systematically explore it to determine the circular frequencies or phase velocities for axisymmetric traveling waves. At roughly the same time period to these circular cylinder studies were the investigations of plane strain vibrations in homogeneous, isotropic plates by Rayleigh (1888) and Lamb (1917). Most of the earlier work was concerned with the spectra for propagating waves. End vibrations were not investigated for about a half century after Rayleigh presented his well-known frequency equation for plane strain vibrations. Much credit for our understanding of end vibrations is due to Mindlin and his colleagues, who were able to define the entire spectra from the Rayleigh–Lamb frequency equation. An account of this development was given by Mindlin (1959). In addition, Onoe et al. (1962), Pao and Mindlin (1960) and Pao (1962) also were able to define the frequency spectra for the axisymmetric and flexural modes of a homogeneous, isotropic circular cylinder. Aside of these geometries, very little data are available for cylinders of other cross-sectional shapes. The monograph of Redwood (1960) contains many references up to its publication date for other cross-sections.

In the two subsequent sections, the mathematical preliminaries are set forth and the governing equations of motion for a cylinder of arbitrary cross-sectional shape and material composition are derived. These equations describe the behavior in which one part is modeled by finite elements and the other is represented analytically. This formulation for general cross-sectional shapes was discussed previously by Dong and Kazic (1989). Then, the tasks of determining the complete spectra for this cylinder are addressed. A two-parameter eigenproblem is generated by substituting the solution waveform into the governing equations in which either the frequency ω or the axial wave number k can serve as the eigenvalue parameter. Adopting the frequency as the eigenvalue parameter gives an eigenproblem for all of the propagating modes. The second eigenproblem with the axial wave number k as the eigenvalue enables all of the end modes of a given frequency ω to be determined. Next, the wave reflection analysis is discussed; it is based on representing the reflected motion by a modal composition of the propagating waves and end modes. A least-squares method or a virtual work method due to Wu and Plunkett (1967) enables the amplitudes of all these modes to be determined. Four cross-sections are studied to illustrate the wave reflection analysis procedure.

2. Preliminaries

Consider a long prismatic cylinder with an arbitrary cross-sectional shape. This cylinder is composed of possible distinct anisotropic materials that are perfectly bonded together along its entire length. Adopt rectangular coordinates (x, y, z) with the z-axis running along its axis and the (x, y) axes spanning its cross-section, and let t denote time. The formulation of the governing equations is based on linear three-dimensional elasticity. The mechanical variables are the displacement $\mathbf{u}$, stress $\boldsymbol{\sigma}$, and strain $\boldsymbol{\varepsilon}$ with components

$$\mathbf{u}(x, y, z) = [u, v, w]^{\mathrm{T}} \tag{1}$$

$$\boldsymbol{\sigma}(x, y, z, t) = [\sigma_{xx}, \sigma_{yy}, \sigma_{zz}, \sigma_{yz}, \sigma_{xz}, \sigma_{xy}]^{\mathrm{T}} \tag{2}$$

$$\boldsymbol{\varepsilon}(x, y, z, t) = [\varepsilon_{xx}, \varepsilon_{yy}, \varepsilon_{zz}, \gamma_{yz}, \gamma_{xz}, \gamma_{xy}]^{\mathrm{T}} \tag{3}$$

In anticipation of the semi-analytical finite element formulation, the linear strain displacement equations are written in split operator form according to differentiations with respect to the cross-sectional variables (x, y) and to the axial coordinate z, i.e.,

$$\boldsymbol{\varepsilon} = \mathbf{L}\mathbf{u} = \left(\mathbf{L}_{xy} + \mathbf{L}_z\right)\mathbf{u} \tag{4}$$

where

$$\mathbf{L}_{xy} = \begin{bmatrix} \frac{\partial}{\partial x} & \cdot & \cdot \\ \cdot & \frac{\partial}{\partial y} & \cdot \\ \cdot & \cdot & \cdot \\ \cdot & \cdot & \frac{\partial}{\partial y} \\ \cdot & \cdot & \frac{\partial}{\partial x} \\ \frac{\partial}{\partial y} & \frac{\partial}{\partial x} & \cdot \end{bmatrix}; \qquad \mathbf{L}_z = \begin{bmatrix} \cdot & \cdot & \cdot \\ \cdot & \cdot & \cdot \\ \cdot & \cdot & \frac{\partial}{\partial z} \\ \cdot & \frac{\partial}{\partial z} & \cdot \\ \frac{\partial}{\partial z} & \cdot & \cdot \\ \cdot & \cdot & \cdot \end{bmatrix} \tag{5}$$

The constitutive relation for each distinct material comprising the prismatic cross-section has the form

$$\boldsymbol{\sigma} = \mathbf{C}\boldsymbol{\varepsilon} \tag{6}$$

where the symmetric (6×6) $\mathbf{C}$ matrix contain the rectilinear elastic, anisotropic moduli.

The governing equations of motion for this beam are derived by Hamilton's principle

$$\delta \int_{t_0}^{t_1} \left\{ T - (U + V_{\mathrm{E}}) \right\} \mathrm{d}t = 0 \tag{7}$$

where T is the kinetic energy, U the strain energy and V_{E} the potential energy of external forces. The kinetic energy in terms of the velocity vector $\dot{\mathbf{u}}$ and unit mass density ρ is of the form

$$T = \frac{1}{2}\int\int\int_B \dot{\mathbf{u}}^{\mathrm{T}}\boldsymbol{\rho}\dot{\mathbf{u}}\,\mathrm{d(vol)} \quad \text{with} \quad \boldsymbol{\rho} = \begin{bmatrix} \rho & \cdot & \cdot \\ \cdot & \rho & \cdot \\ \cdot & \cdot & \rho \end{bmatrix} \tag{8}$$

The strain energy U is given by

$$U = \frac{1}{2}\int\int\int_B \boldsymbol{\varepsilon}^{\mathrm{T}}\mathbf{C}\boldsymbol{\varepsilon}\,\mathrm{d(vol)} \tag{9}$$

The potential energy V_{E} herein consists of applied traction acting on some generic cross-section and it is given by

$$V_{\mathrm{E}} = -\int\int \mathbf{u}^{\mathrm{T}}\boldsymbol{\sigma}_f\,\mathrm{d(surf)} \tag{10}$$

where $\boldsymbol{\sigma}_f$ denotes the normal and shear tractions on the cross-sectional surface.

3. Semi-analytical finite element governing equations

A semi-analytical finite element method is used in our analysis with discretization of bar's cross-section into a system of planar elements. In this semi-analytical finite element version, the axial and time dependencies of the displacement vector $\mathbf{u}$ are regarded as unknowns at the outset, leaving the (x, y) dependence for modeling by interpolation functions. Separation of the dependent variables with one part stated in terms of an assumed field occupies in an intermediate position between an exact solution and a Ritz/Galerkin technique. This procedure is due to Kantorovich and Krylov (1958).

For a generic element of the finite element discretization, the kinematic field takes the form

$$\mathbf{u} = \mathbf{n}(x, y)\mathbf{u}_e(z, t) \tag{11}$$

where $\mathbf{n}$ contain the interpolation functions and $\mathbf{u}_e$ denote the array of nodal displacement variables. In our computer codes for this problem, both six-node triangular and eight-node quadrilateral elements as shown in Fig. 1 are available for modeling the cross-section. Second-order polynomials are used in both types of elements; quadratic interpolations in area coordinates for the triangle and second-order serendipity interpolations for the quadrilateral. In the formulation of the element matrices, isoparametric finite element methodology is used. Since the essence of these interpolations are well documented and the details of Gaussian quadrature for isoparametric element formulations follow a standard well-defined path, the details pertaining to this aspect of the formulations requires no elaboration. In the formulation of the governing equations, only the formal mathematical steps are given.

The substitution eqn (11) into eqn (4) gives deformation measures in terms of the nodal variables as

$$\boldsymbol{\varepsilon} = \mathbf{b}_1\mathbf{u}_e + \mathbf{b}_2\mathbf{u}_{e,z} \tag{12}$$

where

$$\mathbf{b}_1 = \mathbf{L}_{xy}\mathbf{n}(x, y); \quad \mathbf{b}_2 = \mathbf{L}_z\mathbf{n}(x, y) \tag{13}$$

The components of the $\mathbf{b}_1$ and $\mathbf{b}_2$ matrices are

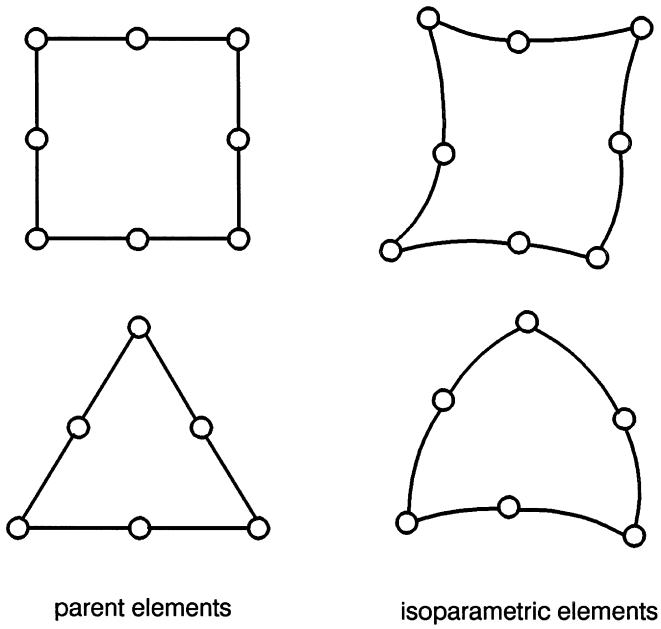

Fig. 1. Diagrams of six-node triangular and eight-node quadrilateral elements.

$$\mathbf{b}_1 = \begin{bmatrix} \mathbf{n}_{,x} & \cdot & \cdot \\ \cdot & \mathbf{n}_{,y} & \cdot \\ \cdot & \cdot & \cdot \\ \cdot & \cdot & \mathbf{n}_{,y} \\ \cdot & \cdot & \mathbf{n}_{,x} \\ \mathbf{n}_{,y} & \mathbf{n}_{,x} & \cdot \end{bmatrix}; \quad \mathbf{b}_2 = \begin{bmatrix} \cdot & \cdot & \cdot \\ \cdot & \cdot & \cdot \\ \cdot & \cdot & \mathbf{n} \\ \cdot & \mathbf{n} & \cdot \\ \mathbf{n} & \cdot & \cdot \\ \cdot & \cdot & \cdot \end{bmatrix} \tag{14}$$

Substituting eqns (11) and (12) into all the energy expressions in Hamilton's principle (7) yields

$$\begin{aligned} \delta \int_{t_0}^{t_1} \Bigg[\frac{1}{2} \int\int\int \Big(& \dot{\mathbf{u}}_e^{\mathrm{T}} \mathbf{n}^{\mathrm{T}} \boldsymbol{\rho} \mathbf{n} \dot{\mathbf{u}}_e - \mathbf{u}_e^{\mathrm{T}} \mathbf{b}_1^{\mathrm{T}} \mathbf{C} \mathbf{b}_1 \mathbf{u}_e - \mathbf{u}_e^{\mathrm{T}} \mathbf{b}_1^{\mathrm{T}} \mathbf{C} \mathbf{b}_2 \mathbf{u}_{e,z} - \mathbf{u}_{e,z}^{\mathrm{T}} \mathbf{b}_2^{\mathrm{T}} \mathbf{C} \mathbf{b}_1 \mathbf{u}_e \\ & - \mathbf{u}_{e,z}^{\mathrm{T}} \mathbf{b}_2^{\mathrm{T}} \mathbf{C} \mathbf{b}_2 \mathbf{u}_{e,z} \Big) \, \mathrm{d}x \, \mathrm{d}y \, \mathrm{d}z + \int\int \mathbf{u}^{\mathrm{T}} \boldsymbol{\sigma}_f \, \mathrm{d}x \, \mathrm{d}y \Bigg] \mathrm{d}t = 0 \end{aligned} \tag{15}$$

Carrying out the integration over the cross-sectional area of the element gives

$$\delta \int_{t_0}^{t_1} \left[\frac{1}{2} \int \left(\dot{\mathbf{u}}_e^{\mathrm{T}} \mathbf{m} \dot{\mathbf{u}}_e - \mathbf{u}_e^{\mathrm{T}} \mathbf{k}_{11} \mathbf{u}_e - \mathbf{u}_e^{\mathrm{T}} \mathbf{k}_{12} \mathbf{u}_{e,z} - \mathbf{u}_{e,z}^{\mathrm{T}} \mathbf{k}_{21} \mathbf{u}_e - \mathbf{u}_{e,z}^{\mathrm{T}} \mathbf{k}_{22} \mathbf{u}_{e,z} \right) \mathrm{d}z + \mathbf{u}_e^{\mathrm{T}} \mathbf{f} \right] \mathrm{d}t = 0 \tag{16}$$

where

$$\mathbf{k}_{11} = \int\int \mathbf{b}_1^{\mathrm{T}} \mathbf{C} \mathbf{b}_1 \, \mathrm{d}x \, \mathrm{d}y; \quad \mathbf{m} = \int\int \mathbf{n}^{\mathrm{T}} \boldsymbol{\rho} \mathbf{n} \, \mathrm{d}x \, \mathrm{d}y$$

$$\mathbf{k}_{12} = \mathbf{k}_{21}^{\mathrm{T}} = \int\int \mathbf{b}_1^{\mathrm{T}}\mathbf{C}\mathbf{b}_2 \,\mathrm{d}x\,\mathrm{d}y; \quad \mathbf{f} = \int\int \mathbf{n}^{\mathrm{T}}\boldsymbol{\sigma}_f \,\mathrm{d}x\,\mathrm{d}y$$

$$\mathbf{k}_{22} = \int \mathbf{b}_2^{\mathrm{T}}\mathbf{C}\mathbf{b}_2 \,\mathrm{d}x\,\mathrm{d}y \tag{17}$$

The total energy for the entire bar is found by summing the energies of the individual elements comprising the model of the cross-section and the counterpart of eqn (16) for the entire cross-section takes the form

$$\delta\int_{t_0}^{t_1}\left[\frac{1}{2}\int\left(\dot{\mathbf{U}}^{\mathrm{T}}\mathbf{M}\dot{\mathbf{U}} - \mathbf{U}^{\mathrm{T}}\mathbf{K}_{11}\mathbf{U} - \mathbf{U}^{\mathrm{T}}\mathbf{K}_{12}\mathbf{U}_z - \mathbf{U}_z^{\mathrm{T}}\mathbf{K}_{21}\mathbf{U} - \mathbf{U}_z^{\mathrm{T}}\mathbf{K}_{22}\mathbf{U}_z\right)\mathrm{d}z + \mathbf{U}^{\mathrm{T}}\mathbf{F}\right]\mathrm{d}t = 0 \tag{18}$$

where $\mathbf{U}$ denotes the assembled nodal variables and the assembled stiffness and mass matrices are merely the superpositions of the N individual element contributions, each of which is denoted by subscript n.

$$\mathbf{K}_{11} = \sum_{n=1}^{N}\mathbf{k}_{11n}; \quad \mathbf{K}_{12} = \mathbf{K}_{21}^{\mathrm{T}} = \sum_{n=1}^{N}\mathbf{k}_{12n}; \quad \mathbf{K}_{22} = \sum_{n=1}^{N}\mathbf{k}_{22n}; \quad \mathbf{M} = \sum_{n=1}^{N}\mathbf{m}_n; \quad \mathbf{F} = \sum_{n=1}^{N}\mathbf{f}_n \tag{19}$$

Since conforming finite elements are used, nodal kinematic continuity assures full inter-element continuity of all elements at common interfaces.

Carrying out the variation indicated by eqn (18) leads to the following governing equation of motion for the anisotropic bar.

$$\mathbf{K}_1\mathbf{U}_{zz} - \mathbf{K}_2\mathbf{U}_z - \mathbf{K}_3\mathbf{U} - \mathbf{M}\ddot{\mathbf{U}} + \mathbf{F} = 0 \tag{20}$$

where

$$\mathbf{K}_3 = \mathbf{K}_{11}; \quad \mathbf{K}_2 = \mathbf{K}_{12} - \mathbf{K}_{21}; \quad \mathbf{K}_1 = \mathbf{K}_{22} \tag{21}$$

Observe that $\mathbf{K}_1$ and $\mathbf{K}_3$ are symmetric and $\mathbf{K}_2$ is antisymmetric. Governing eqn (20) will be used to establish all possible free vibration modes of the bar.

4. Propagating waves and end modes

For free vibrations, suppress the nonhomogeneous term in eqn (20) and seek solutions of the form

$$\mathbf{U} = \mathbf{U}_0\mathrm{e}^{i(\omega t + kz)} \tag{22}$$

where ω is the circular frequency, k is an axial wave number, and $\mathbf{U}_0$ is the vector of nodal displacements. Substituting eqn (22) into the homogeneous form of eqn (20) gives

$$\left[-k^2\mathbf{K}_1 - ik\mathbf{K}_2 - K_3 + \omega^2\mathbf{M}\right]\mathbf{U}_0\mathrm{e}^{i(\omega t + kz)} = 0 \tag{23}$$

As the exponential factor does not vanish for all z and t, then

$$\left[k^2\mathbf{K}_1 + ik\mathbf{K}_2 + \mathbf{K}_3 - \omega^2\mathbf{M}\right]\mathbf{U}_0 = 0 \tag{24}$$

which is an algebraic eigenproblem where either ω^2 or k may be assigned the role of eigenvalue. These two cases of ω^2 or k as the eigenvalue are discussed as follows.

4.1. Propagating waves

By assigning real values to k and taking ω^2 as the eigenvalue, eqn (24) admits eigendata for the propagating or traveling waves. Due to the symmetric and antisymmetric characteristics of the stiffness matrices $\mathbf{k}_i$s, eqn (24) is a hermitian system which guarantees real ω^2s as eigenvalues. Its complex nature can be rendered real by recasting it as

$$\mathbf{K}_T\mathbf{V}_0 = \omega^2\mathbf{M}_T\mathbf{V}_0 \tag{25}$$

where

$$\mathbf{V}_0 = \begin{bmatrix} \mathbf{U}_0 \\ -i\mathbf{U}_0 \end{bmatrix}; \quad \mathbf{K}_T = \begin{bmatrix} \mathbf{K}_3 + k^2\mathbf{K}_1 & -k\mathbf{K}_2 \\ k\mathbf{K}_2 & \mathbf{K}_3 + k^2\mathbf{K}_1 \end{bmatrix}; \quad \mathbf{M}_T = \begin{bmatrix} \mathbf{M} & \cdot \\ \cdot & \mathbf{M} \end{bmatrix} \tag{26}$$

Note that both $\mathbf{K}_T$ and $\mathbf{M}_T$ are symmetric and positive-definite. The solution to eqn (25) may be stated as a transformation to normal coordinates $\mathbf{x}$.

$$\mathbf{V}_0 = \mathbf{\Phi}\mathbf{x} \tag{27}$$

where $\mathbf{\Phi}$ is the modal matrix. The columns of $\mathbf{\Phi}$ satisfy the following orthogonality conditions.

$$\phi_m^H\mathbf{M}_T\phi_n = \delta_{mn}; \quad \phi_m^H\mathbf{K}_T\phi_n = \delta_{mn}\omega_n^2 \tag{28}$$

with superscript H denoting conjugate transpose. Based on the form of $\mathbf{V}_0$ in eqn (26), the roles of the real and imaginary parts of the upper half of the modal matrix $\mathbf{\Phi}$ are interchanged in the lower half. But since an eigenvector is determined within an arbitrary constant, then without loss of generality, the upper and lower halves of the modal matrix $\mathbf{\Phi}$ can be cast as the real and imaginary parts of the eigensolution of $\mathbf{U}_0$, i.e., $\mathbf{U}_0 = (\mathbf{\Phi}_r + i\mathbf{\Phi}_i)\mathbf{x}$ or

$$\mathbf{V}_0 = \begin{bmatrix} \mathbf{\Phi}_U \\ \mathbf{\Phi}_L \end{bmatrix}\mathbf{x} = \begin{bmatrix} \mathbf{\Phi}_r \\ \mathbf{\Phi}_i \end{bmatrix}\mathbf{x} \tag{29}$$

Orthogonality relations (28) expressed in terms of real and imaginary parts of any two columns (ϕ_{rm}, ϕ_{im}) and (ϕ_{rn}, ϕ_{in}) of $(\mathbf{\Phi}_r, \mathbf{\Phi}_i)$ and the mass and stiffness matrices $\mathbf{M}$ and $\mathbf{K}_i$s take the form

$$\phi_{rm}^{\mathrm{T}}\mathbf{M}\phi_{rn} + \phi_{im}^{\mathrm{T}}\mathbf{M}\phi_{in} = \delta_{mn}$$

$$\phi_{rm}^{\mathrm{T}}\left(\mathbf{K}_3 + k^2\mathbf{K}_1\right)\phi_{rn} + \phi_{im}^{\mathrm{T}}\left(\mathbf{K}_3 + k^2\mathbf{K}_1\right)\phi_{in} + k\left(\phi_{im}^{\mathrm{T}}\mathbf{K}_2\phi_{rn} - \phi_{rm}^{\mathrm{T}}\mathbf{K}_2\phi_{in}\right) = \delta_{mn}\omega_n^2 \tag{30}$$

Eigensystem (25) yields ω_i^2 in pairs, the eigenvectors of which are distinct, but they represent identical waveforms that are separated by a $\pi/2$ phase. By systematically varying k over a range of real wave numbers, eigensystem (25) establishes the dispersion relation for the bar.

4.2. End modes

If ω^2 is assigned values in algebraic eigensystem (24), k becomes the eigenvalue. To render the eigensystem completely real, set

$$k = -i\gamma \tag{31}$$

in eqn (24) and it becomes a quadratic eigenvalue problem

$$\gamma^2\mathbf{K}_1\mathbf{U}_0 - \gamma\mathbf{K}_2\mathbf{U}_0 - \left(\mathbf{K}_3 - \omega^2\mathbf{M}\right)\mathbf{U}_0 = 0 \tag{32}$$

This equation may be reduced to first-order form by introducing an auxiliary variable $\mathbf{U}_1$ as

$$\mathbf{U}_1 = \gamma\mathbf{U}_0 \tag{33}$$

With this auxiliary variable, the algebraic eigensystem can be recast as

$$\mathbf{AV} = \gamma\mathbf{BV} \tag{34}$$

where

$$\mathbf{V} = \begin{bmatrix} \mathbf{U}_0 \\ \mathbf{U}_1 \end{bmatrix} = \begin{bmatrix} \mathbf{U}_0 \\ \gamma\mathbf{U}_0 \end{bmatrix};$$

$$\mathbf{A} = \begin{bmatrix} \cdot & \mathbf{K}_3 - \omega^2\mathbf{M} \\ \mathbf{K}_3 - \omega^2\mathbf{M} & \mathbf{K}_2 \end{bmatrix}; \quad \mathbf{B} = \begin{bmatrix} \mathbf{K}_3 - \omega^2\mathbf{M} & \cdot \\ \cdot & \mathbf{K}_1 \end{bmatrix} \tag{35}$$

Eigenproblem (34) admits both real and complex eigenvalues that describe end modes whose vibratory amplitudes decay exponentially into its interior from the free end of a semi-infinitely long cylinder. Real eigenvalues γs occur in pairs $(\pm\gamma_r)$, and they decay monotonically in the $\mp z$-directions. Complex eigenvalues γs occur in complex conjugate pairs $(\pm\gamma_r \pm i\gamma_i)$ and they decay sinusoidally in the $\mp z$-directions. There is an exceptional case where γs occur as a purely imaginary pair $(\gamma = \pm i\gamma_i)$, and these roots represent propagating waves and do not fit the definition of an end mode. Nevertheless, eigensystem (34) admits a finite number of them for any given ω^2. In view of eqn (31), the real and imaginary parts of the eigenvalue γ in terms of k are

$$k = \pm\gamma_i \mp i\gamma_r \tag{36}$$

For each eigenvalue $\gamma_m = ik_m$ of eqn (34), there are right-handed and left-handed eigenvectors, ϕ_m and $\psi_{m,}$ respectively, that satisfy

$$\left[\mathbf{A}(\omega) - ik_m\mathbf{B}\right]\phi_m = 0; \quad \left[\mathbf{A}^{\mathrm{T}}(\omega) - ik_m\mathbf{B}\right]\psi_m = \mathbf{0} \tag{37}$$

These eigenvectors satisfy the bi-orthogonality relations

$$\mathbf{\Psi}^{\mathrm{T}}\mathbf{B}\mathbf{\Phi} = \mathrm{diag}(B_n); \quad \mathbf{\Psi}^{\mathrm{T}}\mathbf{A}\mathbf{\Phi} = \mathrm{diag}(B_n ik_n) \tag{38}$$

In view of eqn (35) defining the lower half of $\mathbf{V}$ as the product of the eigenvalue and its upper half, each set of right-handed and left-handed eigenvectors can be expressed completely in terms of its upper half eigenvectors (ϕ_{um}, ψ_{um}) and eigenvalue as

$$\phi_m = \begin{bmatrix} \phi_{um} \\ \text{----------} \\ ik_m\phi_{um} \end{bmatrix}; \quad \psi_m = \begin{bmatrix} \psi_{um} \\ \text{----------} \\ ik_m\psi_{um} \end{bmatrix} \tag{39}$$

Then, bi-orthogonality relations (38) take the form

$$\psi_{um}^{\mathrm{T}}\left(\mathbf{K}_3 - \omega^2\mathbf{M}\right)\phi_{un} - k_m k_n \psi_{um}^{\mathrm{T}}\mathbf{K}_1\phi_{un} = \delta_{mn}B_n$$

$$(ik_n + ik_m)\psi_{um}^{\mathrm{T}}\left(\mathbf{K}_3 - \omega^2\mathbf{M}\right)\phi_{un} - k_m k_n \psi_{um}^{\mathrm{T}}\mathbf{K}_2\phi_{un} = \delta_{mn}B_n ik_n \tag{40}$$

5. Reflection of traveling wave

Consider a semi-infinitely long bar occupying the region ($z \le 0$) with the cross-sectional plane $z = 0$ traction-free. Let a monochromatic wave train of frequency ω advance from $z = -\infty$ toward the origin. The wave form of the incident wave is

$$\mathbf{U}_{\mathrm{inc}}(z, t) \equiv \mathbf{U}_{\mathrm{inc}}(z)\, \mathrm{e}^{i\omega t} = A_{\mathrm{inc}}\mathbf{U}_0\, \mathrm{e}^{-ik_{\mathrm{inc}}z}\, \mathrm{e}^{i\omega t} \tag{41}$$

where $\mathbf{U}_0 = \phi_{un(\mathrm{inc})}$ is a right-handed eigenvector representing an admissible propagating mode with amplitude A_{inc} and wave number k_{inc}. Its arrival at the traction-free end causes a reflection phenomenon that may involve one or more opposite traveling waves as well as a host of end modes. Both types of motions are needed to satisfy traction-free end conditions. Of the complete set of eigenmodes discussed in the previous section, only half are admissible in the end reflection problem for the region ($z \le 0$), i.e., those of the products ik_ns whose real part is positive. The products ik_ns with negative real part involve motions exhibiting exponential growth in the negative z-direction and must therefore be suppressed in order to bound the displacements at $z = -\infty$. In what follows, the exponential time factor $\mathrm{e}^{i\omega t}$ is omitted without loss of generality.

Let the reflected motion be written in terms of the upper right-handed eigenvectors of eqn (39) as

$$\mathbf{U}_{\mathrm{ref}}(z) = \sum_{n=1}^{N} A_n \phi_{un} \mathrm{e}^{ik_n z} \tag{42}$$

where all admissible propagating waves and end modes are included in the sum and A_ns denote the undetermined coefficients of the reflected modes. Evaluating eqn (42) at $z = 0$ gives

$$\mathbf{U}_{\mathrm{ref}}|_{z=0} = \mathbf{GA} \tag{43}$$

where the columns of $\mathbf{G}$ are

$$\mathbf{G} = \left[\phi_{u1}, \phi_{u2}, \phi_{u3}, \ldots, \phi_{uN}\right] \tag{44}$$

$$\mathbf{A}^{\mathrm{T}} = [A_1, A_2, A_3, \ldots, A_N] \tag{45}$$

The sum of the stresses of the incident wave and reflected motion must be zero for a traction-free surface $z = 0$. The relevant stress components at discrete points on the free surface due to the reflected motion, which are based on eigenvectors $\mathbf{\Phi}_u$s, are evaluated using strain–displacement relation (12) and constitutive law (6). They are denoted by

$$\mathbf{R}_{\mathrm{ref}}|_{z=0} = -\mathbf{FA} \tag{46}$$

where $\mathbf{F}$ contain the modal columns $\mathbf{f}_j$s

$$\mathbf{F} = [\mathbf{f}_1, \mathbf{f}_2, \mathbf{f}_3, \ldots, \mathbf{f}_N] \tag{47}$$

with each $\mathbf{f}_j$ denoting the following traction components.

$$\mathbf{f}_j^{\mathrm{T}} = [\sigma_{xz1j}, \sigma_{yz1j}, \sigma_{zz1j}, \sigma_{xz2j}, \sigma_{yz2j}, \sigma_{zz2j}, \ldots, \sigma_{xzNj}, \sigma_{yzNj}, \sigma_{zzNj}] \tag{48}$$

The surface stresses due to the incident wave on the plane $z = 0$ are therefore

$$\mathbf{R}_{\text{inc}}|_{z=0} = \mathbf{F}_{\text{inc}}\mathbf{A}_{\text{inc}} \tag{49}$$

The coefficients **A**s are calculating by insisting that the surface stresses of both incident wave and the reflected motion vanish on the plane $z = 0$.

$$\mathbf{R} \equiv \mathbf{R}_{\text{inc}}|_{z=0} + \mathbf{R}_{\text{ref}}|_{z=0} = 0 \rightarrow \mathbf{F}_{\text{inc}}\mathbf{A}_{\text{inc}} - \mathbf{F}\mathbf{A} = 0 \tag{50}$$

Wu and Plunkett (1967) presented two methods for determining these coefficients.

5.1. Minimization of the residual boundary values

This is a least-squares method in which a norm is defined. The solution for the coefficients take the form

$$\mathbf{A} = \mathbf{A}_{\text{inc}}\left[\int \mathbf{F}^H\mathbf{F}\,\mathrm{d}A\right]^{-1}\left[\int \mathbf{F}^H\mathbf{F}_{\text{inc}}\,\mathrm{d}A\right] \tag{51}$$

5.2. Virtual work method

By enforcing the virtual work on the free end, i.e.,

$$\delta\mathbf{U}^H\mathbf{R} = 0 \tag{52}$$

where

$$\mathbf{U} = \mathbf{U}_{\text{inc}}|_{z=0} + \mathbf{U}_{\text{ref}}|_{z=0} \tag{53}$$

so that the variation of **U** involves only the reflected motion, i.e.,

$$\delta\mathbf{U} \equiv \delta\mathbf{U}_{\text{ref}} \tag{54}$$

Substituting eqn (54) into the virtual work expression (52) gives

$$\mathbf{A} = \mathbf{A}_{\text{inc}}\left[\int \mathbf{G}^H\mathbf{F}\,\mathrm{d}A\right]^{-1}\left[\int \mathbf{G}^H\mathbf{F}_{\text{inc}}\,\mathrm{d}A\right] \tag{55}$$

In carrying out the end conditions, the stresses and displacements are evaluated at the same Gaussian quadrature points at those used in the formation of the element matrices.

6. Energy conservation

The sum of the time-average values of energy flux of the reflected traveling waves must be equal to that of the incident wave. The conservation principle can be used to measure the accuracy of the amplitude coefficients of the reflected motion. Note that only propagating waves are capable of transporting energy into the interior of the bar.

The time-average energy flux E_j for the j-th traveling wave and that of the incident wave E_{inc} are given by

$$E_j = i\left[\omega|\mathbf{A}_j|^2 \int \mathbf{f}_j^{\mathrm{T}} \bar{\phi}_{uj}\, \mathrm{d}A\right]; \quad j = 1, 2, \ldots, N_p \tag{56}$$

$$E_{\mathrm{inc}} = i\left[\omega|\mathbf{A}_{\mathrm{inc}}|^2 \int \mathbf{F}_i^{\mathrm{T}} \bar{\mathbf{U}}_0\, \mathrm{d}A\right] \equiv \mathrm{Im}\left[\omega|\mathbf{A}_{\mathrm{inc}}|^2 \int \mathbf{F}_i^{\mathrm{T}} \bar{\phi}_{u(\mathrm{inc})}\, \mathrm{d}A\right] \tag{57}$$

where an over-bar indicates complex conjugation and N_p denotes the number of propagating waves. It is noted that the calculation of the energy flux by eqn (56) with a propagating wave will result in a real value for the flux. Using an end mode in the same formula yields a purely imaginary or complex value for k, as end modes conduct no net energy flux into the interior of the bar.

The total energy flux of the reflected traveling waves is therefore

$$E_{\mathrm{ref}} = \sum_{j=1}^{N_p} E_j \tag{58}$$

Energy conservation requires that $E_{\mathrm{inc}} = E_{\mathrm{ref}}$, so that

$$\sum_{j=1}^{N_p} E_j = E_{\mathrm{inc}} \quad \text{or} \quad \sum_{j=1}^{N_p} \frac{E_j}{E_{\mathrm{inc}}} = 1 \tag{59}$$

A calculation of this type can be used to measure the accuracy of the analysis.

7. Analysis of various cross-sectional geometries

To illustrate wave reflection calculations, four different cross-sectional geometries were considered. The properties and geometries of the are summarized as follows.

1. Homogeneous, isotropic solid circular cylinder; Poisson's ratio $\nu = 0.25$, and radius R.
2. Homogeneous, isotropic rectangular bar; Poisson's ratio $\nu = 0.30$, and height to width ratio $H/W = 1/2$.
3. Three layer $+30^\circ/-30^\circ/+30^\circ$ fiber composite rectangular bar; height to width ratio $H/W = 1/2$ with properties given by eqn (60).
4. Two layer $\pm 30^\circ$ fiber composite rectangular bar; height to width ratio $H/W = 1/2$ with properties given by eqn (60).

These cross-sections are shown in Fig. 2; on the left side are the cross-sectional shapes and on the right side are the finite element models with the total number of corner and mid-side nodes indicated. The fiber composite material properties of cross-sections (3) and (4) are

$$E_L = 139.274\ \mathrm{GPa}; \quad E_t = 15.167\ \mathrm{GPa};$$

$$G_{LT} = 5.861\ \mathrm{GPa}; \quad G_{TT} = 6.268\ \mathrm{GPa}; \quad \nu_{LT} = \nu_{TT} = 0.21 \tag{60}$$

The corresponding elastic moduli in $\mathbf{C}$ at fiber orientations of $\pm 30^\circ$ with respect to the z-axis are

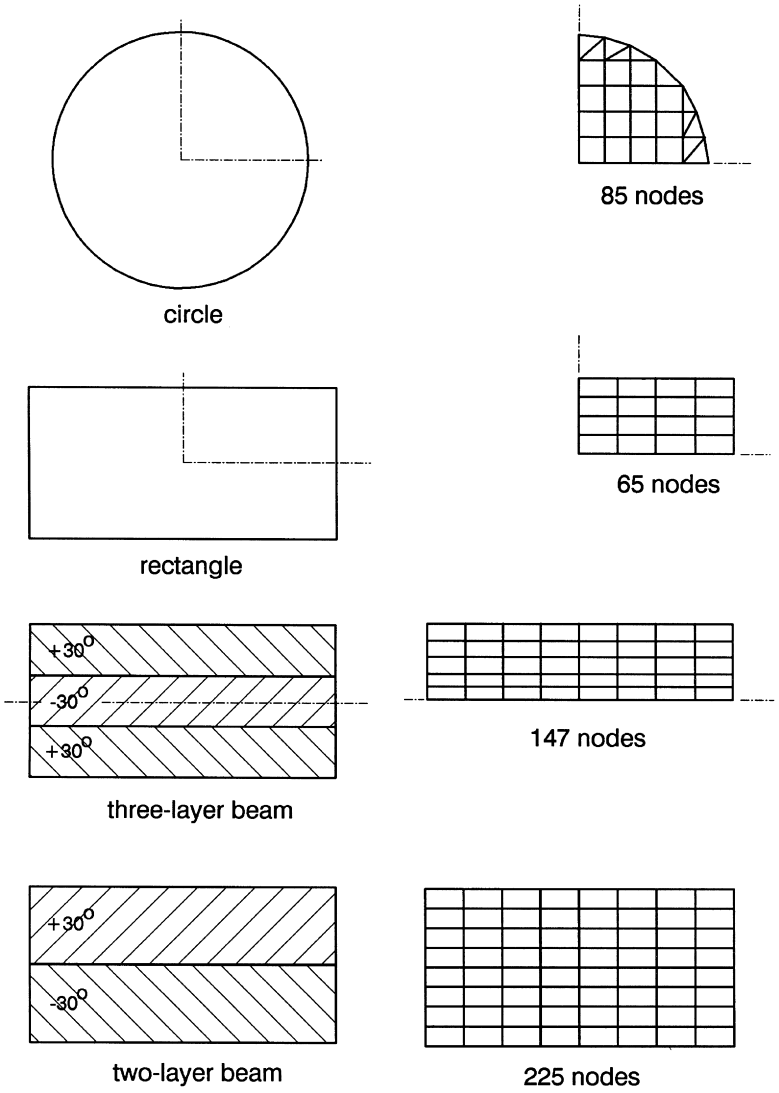

Fig. 2. Diagrams and finite element models of the four examples.

$$[C]_{\pm 30^\circ} = \begin{bmatrix} 15.9860 & 3.6078 & 3.9233 & \mp 0.2732 & \cdot & \cdot \\ 3.6078 & 23.7300 & 27.5875 & \mp 13.4923 & \cdot & \cdot \\ 3.9233 & 27.5875 & 86.2310 & \mp 40.6352 & \cdot & \cdot \\ \mp 0.2732 & \mp 13.4923 & \mp 40.6352 & 29.3675 & \cdot & \cdot \\ \cdot & \cdot & \cdot & \cdot & 5.9628 & \cdot \\ \cdot & \cdot & \cdot & \cdot & \cdot & 6.1663 \end{bmatrix}_{\text{GPa}} \tag{61}$$

All results are presented in term of a normalized frequency Ω and a dimensionless wave number $\bar{k}$ given

by

$$\Omega = \frac{\omega}{\omega_{\text{ref}}}; \quad \bar{k} = kL_{\text{typi}} \tag{62}$$

where ω_{ref} is the reference frequency and L_{typi} denotes a characteristic dimension of the cross-section. The reference frequency and typical length L_{typi} for the four cross-sections are

	(1)	(2)	(3)	(4)
Cross-section	Circle	Rectangle	Three layer beam	Two layer beam
ω_{ref}^2	$(\lambda+2\mu)/\rho R^2$	$\mu/\rho H^2$	$E_T/\rho H^2$	$E_T/\rho H^2$
L_{typi}	R	H	H	H

7.1. Homogeneous, isotropic, solid circular cylinder

This configuration was considered because abundant extant data enable us to assess the accuracy of the present results. Axisymmetric spectral data for both propagating modes and end vibrations were first given by Onoe et al. (1962), and flexural spectral data were presented by Pao and Mindlin (1960) and Pao (1962). The axisymmetric wave reflection problem was studied analytically by Gregory and Gladwell (1989) and by means of 1-D semi-analytical finite elements by Rattanawangchareon et al. (1994). Present axisymmetric wave reflection results, based on 2-D finite element capabilities, were compared with those in these two references. Flexural wave reflection results are also given; but to the best of the author's knowledge, no such results as yet have appeared.

One-quarter of the circular cross-section was modeled as shown in Fig. 2. Doubly symmetric interface conditions must be enforced on the two orthogonal structural planes for axisymmetric motions. In contrast, for flexural motions, symmetry/antisymmetry interface conditions are required. It is mentioned that for circular geometries, cylindrical coordinates are normally used. The axisymmetric and flexural results of the Gregory and Gladwell (1989) and Rattanawangchareon et al. (1994) are given in terms of cylindrical coordinates, i.e., for circumferential mode number $n = 0$ and $n = 1$. Herein, the computer code can treat general two-dimensional cross-sections; the finite element model with either symmetry/symmetry or symmetry/antisymmetry interface conditions are capable of admitting other behaviors exhibiting these conditions in addition to the axisymmetric and flexural motions.

The spectral branches for lowest seven propagating modes extracted from eqn (25) using doubly symmetric interface conditions are shown in Fig. 3 (the sym–sym plot). Of these seven modes, only three are axisymmetric (i.e., $n = 0$) while the others are spectral curves for circumferential mode numbers $n = 2, 4$. These modes are admissible because they also satisfy symmetry/symmetry interface conditions, but they should not be excited by an incident axisymmetric wave. In all calculations, the lowest axisymmetric mode was adopted as the incident wave. The energy distribution of the various reflected propagating modes is shown in Fig. 4 (the sym–sym plot) for normalized frequency range ($1.8 \leq \mathbf{\Omega} \leq 2.4$), i.e., the same used by Gregory and Gladwell (1989) and Rattanawangchareon et al. (1994). Fifty end modes based on eqn (34) together with all of the admissible propagating modes (including those modes with $n = 2, 4$) were used in the calculation of the amplitudes of the reflected modes and energy fluxes. The broken vertical lines in Fig. 4 marks the frequency where an additional propagating wave can be cut on. There is good visual agreement between the present results in Fig. 4 with those of Gregory and Gladwell (1989) and Rattanawangchareon et al. (1994). Even though non-

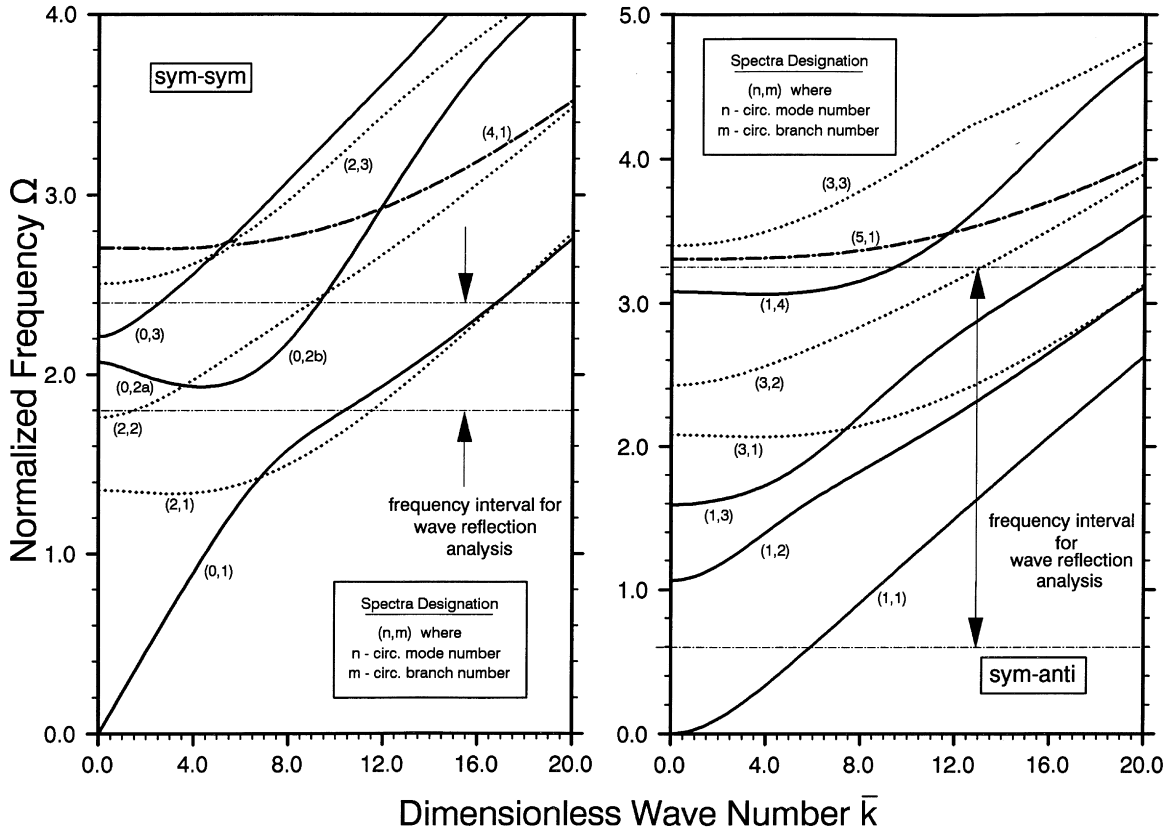

Fig. 3. Frequency spectra for homogeneous, isotropic, circular cylinder.

axisymmetric modes, $n = 2, 4$, were submitted to the analysis procedure for representing the reflected motion, none of them were selected as their computed amplitudes were essentially zero. Observe that as frequencies approached regions where an additional propagating wave can be cut on, the energy flux lines behave quite dramatically. It is mentioned that ten end modes were sufficient to capture the behavior in this frequency range with the virtual work method. By least squares, the comparable accuracy required essentially all fifty end modes. The same observation was made by Rattanawangchareon et al. (1994). It is noted that for a spectral branch with a dip where the slope is negative, such as the portion $(0, 2a)$ of the branch designated as $(0, 2a)$ and $(0, 2b)$ of Fig. 3, the group velocity is negative. In this situation, the data from the mirror image branch (i.e., the one symmetric about the frequency axis) must be used. This situation also occurs in the other examples.

The lowest eight spectral branches with symmetry/antisymmetry interface conditions are shown in Fig. 3 (the anti-sym plot). In this case, four of them are not flexural, i.e., they are not for $n = 1$ but for circumferential mode numbers $n = 3, 5$, which are admissible since they also satisfy symmetry/antisymmetry interface conditions. Using the lowest flexural mode as the incident wave, the energy distribution of the reflected traveling waves in the frequency range $(0.6 \leq \Omega \leq 3.3)$ is plotted in Fig. 4 (the anti-sym plot). Again, the analysis procedure did not select any of the propagating waves with circumferential mode numbers $n = 3, 5$ for the reflected motion.

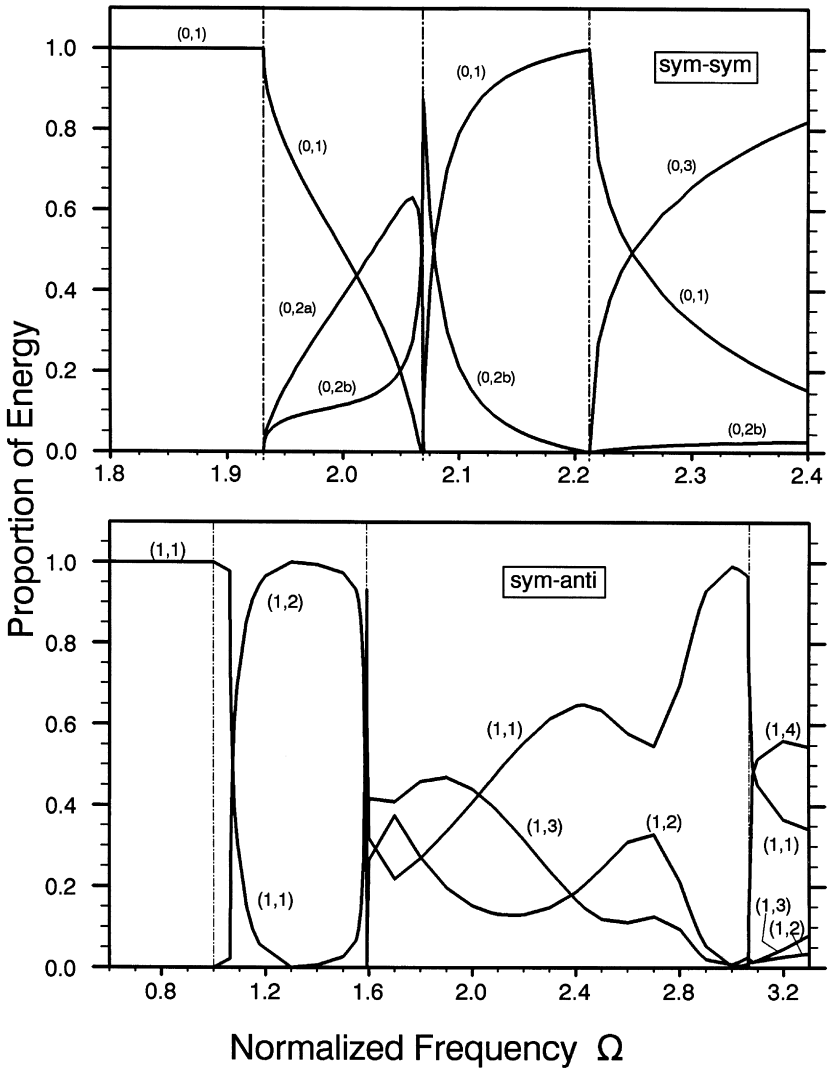

Fig. 4. Energy distributions in reflected waves for homogeneous, isotropic circular cylinder.

7.2. Homogeneous, isotropic, rectangular bar

For a homogeneous, isotropic rectangular bar with height to width ratio $H/W = 1/2$, only one fourth of it requires discretization as shown in Fig. 2 due to its doubly symmetric geometry. Imposing various combinations of symmetry/antisymmetry interface conditions on these two symmetry planes decomposes the total problem into four separate and uncoupled waveforms: (1) extension (sym/sym), (2) and (3) flexure (sym/antisym and antisym/sym) about the two principal axes and (4) torsion (antisym/antisym).

For the rectangular cross-section, the only available analytical spectral data are that for propagating waves; see Kynch (1957), Nigro (1966) and Fraser (1969). Finite element results for propagating waves

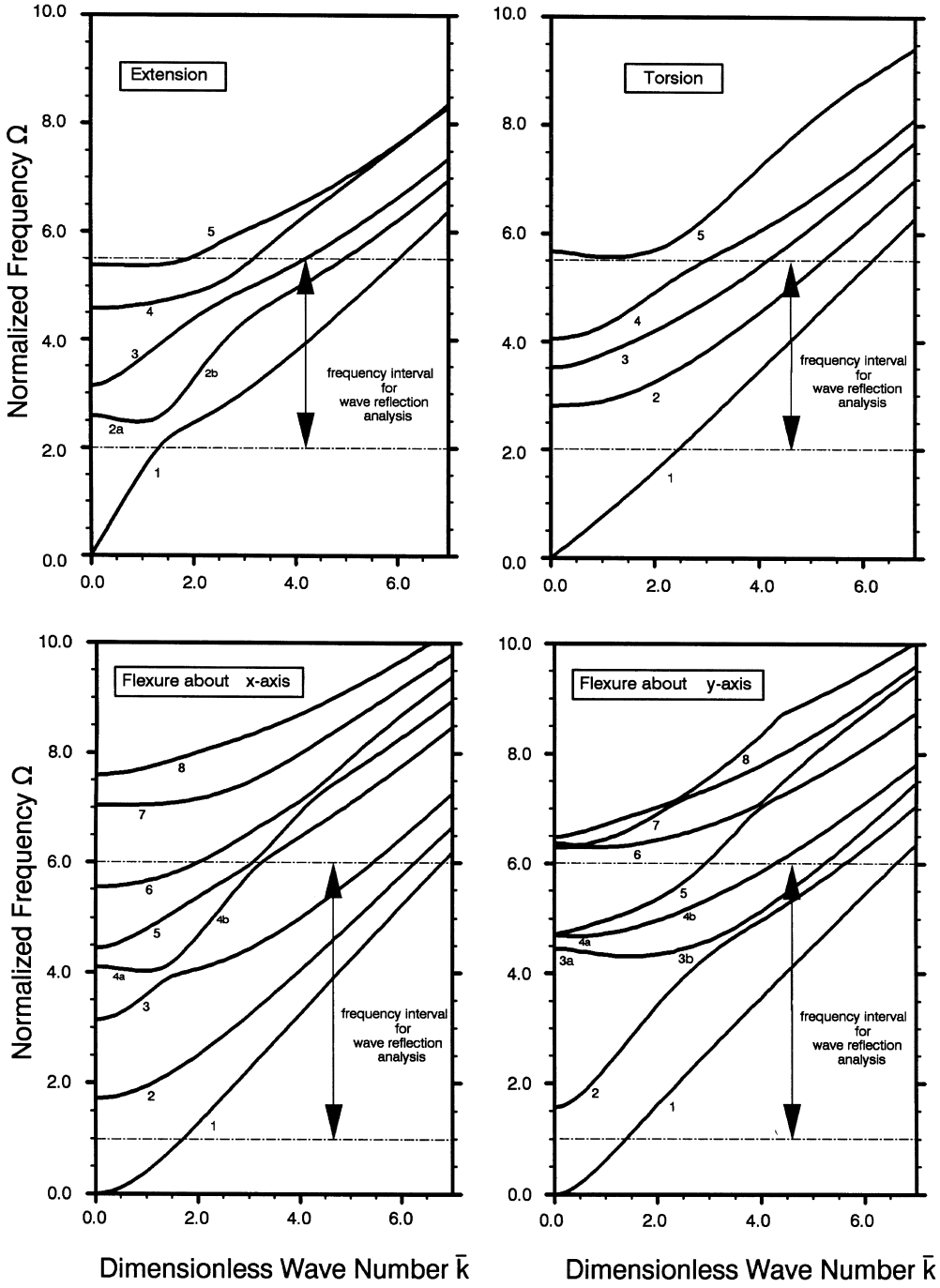

Fig. 5. Frequency spectra for homogeneous, isotropic rectangular cylinder.

were first given by Aalami (1973). Dong and Kazic (1989) gave some end vibration data for extensional motions in a homogeneous, isotropic square bar; their results were based on semi-analytical two-dimensional finite elements (i.e., same as the present formulation). Beyond these investigations, there does not appear to be any other data.

Frequency spectra for lowest propagating modes of these four waveforms (extensional, flexural and torsional waves) are shown in Fig. 5. On these plots are marked the frequency ranges that are under consideration in the reflection problems. In each case, the lowest traveling wave in each of the four waveforms was taken as the incident wave and fifty end modes were used. The reflection results in the form of division of energies in the various reflected traveling waves are presented in Fig. 6a for extensional and torsional motions in the range ($2.0 \leq \Omega \leq 5.5$) and Fig. 6b for the two flexural motions

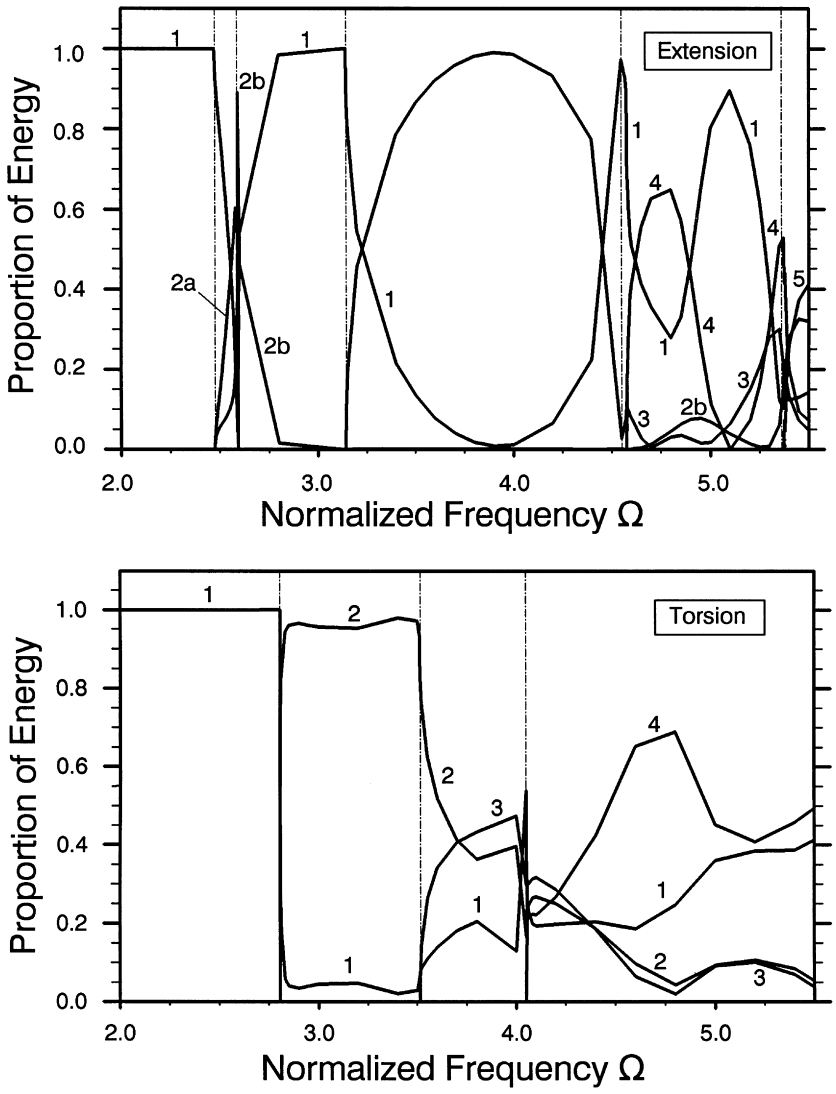

Fig. 6a. Energy distributions in reflected extensional and torsional waves in homogeneous, isotropic rectangular cylinder.

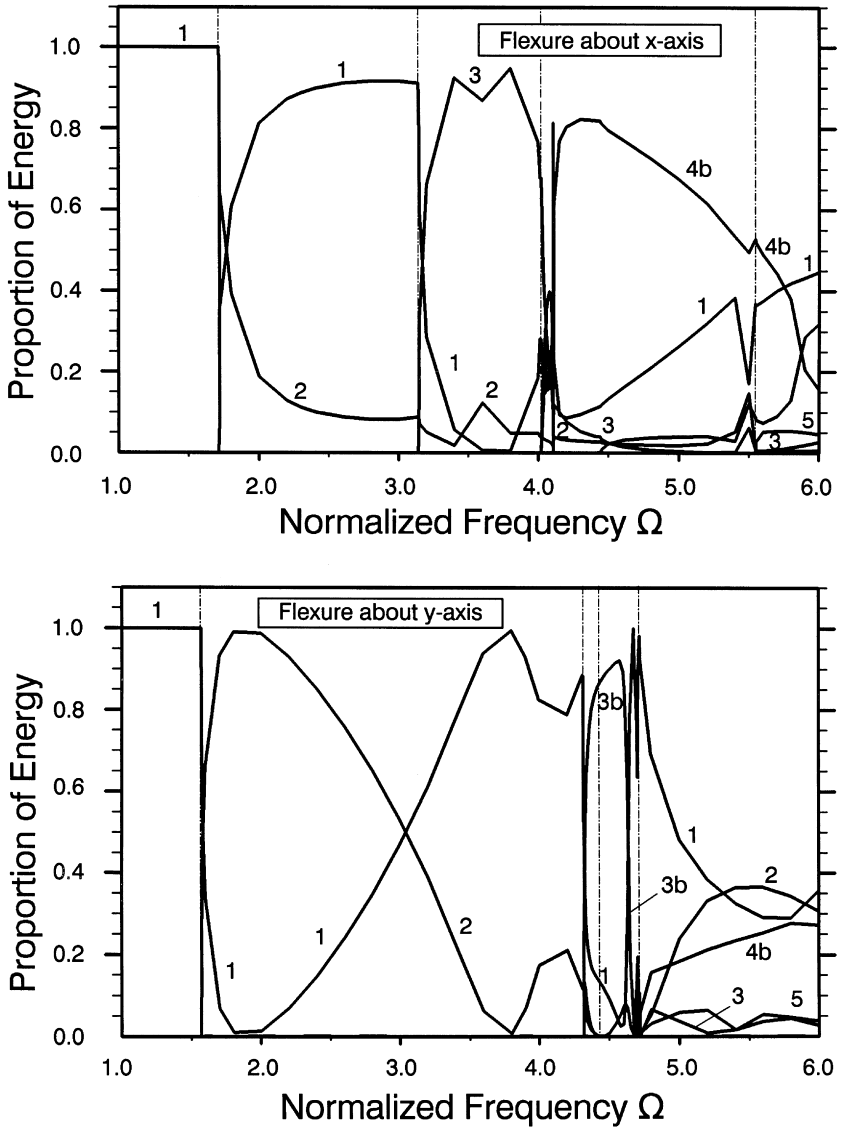

Fig. 6b. Energy distributions in reflected flexural waves in homogeneous, isotropic rectangular cylinder.

$(1.0 \leq \Omega \leq 6.0)$. Enlarged portions of the plots in Fig. 6b where the various curves are crowded are given in Fig. 7 in the ranges of $(3.9 \leq \Omega \leq 4.2)$ and $(4.2 \leq \Omega \leq 4.8)$ in order to show the reflected flexural energy distributions more clearly. Again, the broken vertical lines in the reflected energy distributions marks the frequency at which another propagating wave can be cut on.

7.3. Three layer $+30^\circ/-30^\circ/+30^\circ$ fiber composite rectangular bar

For three layer rectangular bar with an overall height-to-width ratio of $H/W = 1/2$ shown in Fig. 2 with properties given by eqn (61), the horizontal mid-plane is a symmetry plane. Thus, only half of the

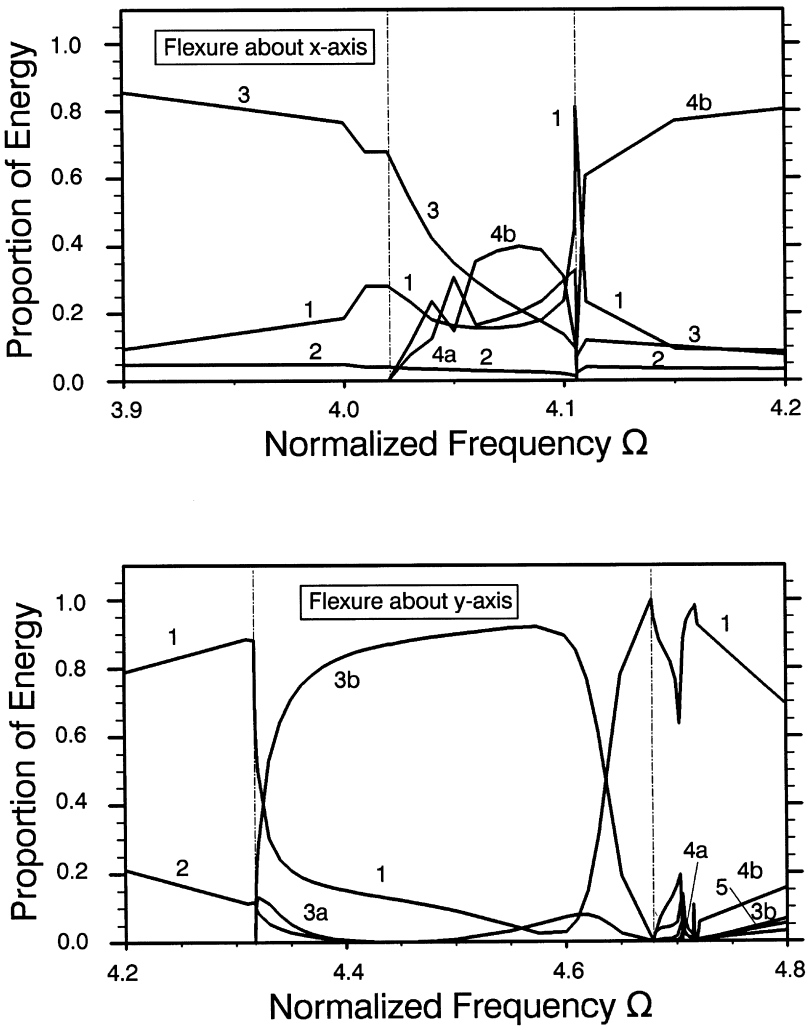

Fig. 7. Enlarged views of energy distributions in reflected flexural waves in homogeneous, isotropic rectangular cylinder.

cross-section requires discretization as shown in Fig. 2. Symmetric and antisymmetric motions with respect to the horizontal mid-plane can be studied separately by imposing symmetry and antisymmetry displacement conditions about it.

Symmetric motions about the horizontal mid-plane include extensional waves and flexural waves about the y-axis. In this cross-sectional profile, these two waveforms are coupled, i.e., they cannot occur independently of each other. The frequency spectra of the symmetric modes are shown in Fig. 8. In labeling the lowest two branches, the descriptors bend–ext and ext–bend were used, in which the first term in the hyphenated expression designates the predominant behavior of that branch. The higher modes also exhibit coupling, but no attempt was made here to assign labels to them in accordance to their predominant characteristics. In the higher modes, their waveforms are somewhat intricate and it is not a straightforward matter to identify their predominant behavior from the displacement modal pattern. Therefore, they are just numbered sequentially. In the wave reflection studies, two cases of

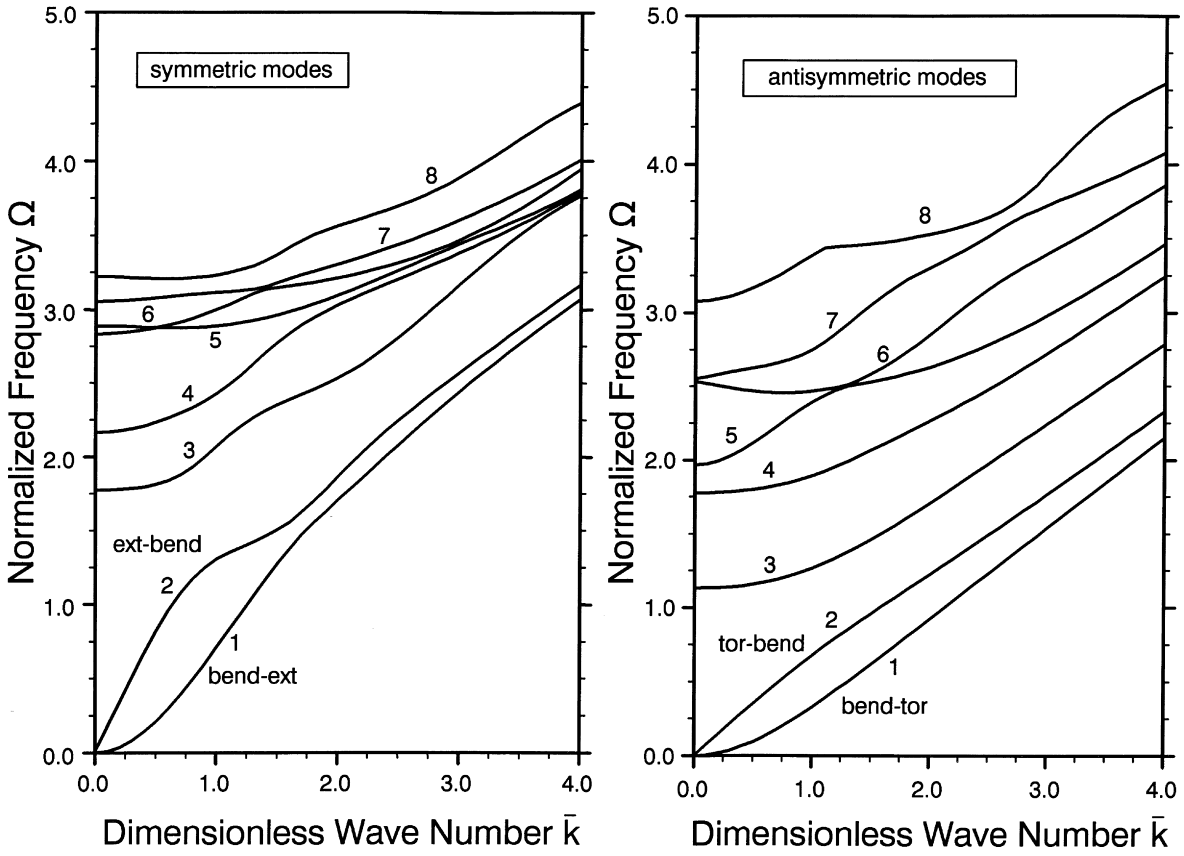

Fig. 8. Frequency spectra for three layer [+30/−30/+30] composite material cylinder.

incident waves were considered using one of the two lowest waveforms, viz, (1) first (bend–ext) mode and (2) second (ext–bend) mode. Depending on the frequency, 100–150 end modes were used. The reflected energy distribution over the frequency range ($0 \leq \Omega \leq 2.25$) with the first mode as the incident wave is shown in Fig. 9a and that with the second mode as the incident wave in Fig. 9b. Upon comparing Fig. 9a with Fig. 9b, it is seen that the reflected energy distributions in both cases for frequencies below the third mode cut on frequency, i.e., that marked by the broken vertical line at $\Omega \approx 1.12$, are reciprocals of each other. In other words, the amount of reflection energy in second mode when excited by the first mode as the incident wave is the same as that in the first mode with the second mode as the incident wave. Above the third mode cut on frequency, the reflected energy distributions for these two cases are distinct.

Antisymmetric motions about the horizontal mid-plane include the torsional waves and flexural waves about the x-axis, and both of these behaviors are coupled. Much of the antisymmetric behavior is the complement of the symmetric behaviors. The frequency spectra are shown in Fig. 8. Following the same labeling convention, the lowest two branches of the frequency spectra are denote as bend–tor and tor–bend according to the predominant characteristics of each branch. All the antisymmetric higher modes are numbered sequentially. Again, the lowest two modes were taken separately as incident waves, and depending on the frequency one hundred to one hundred fifty end modes were used in the calculation of

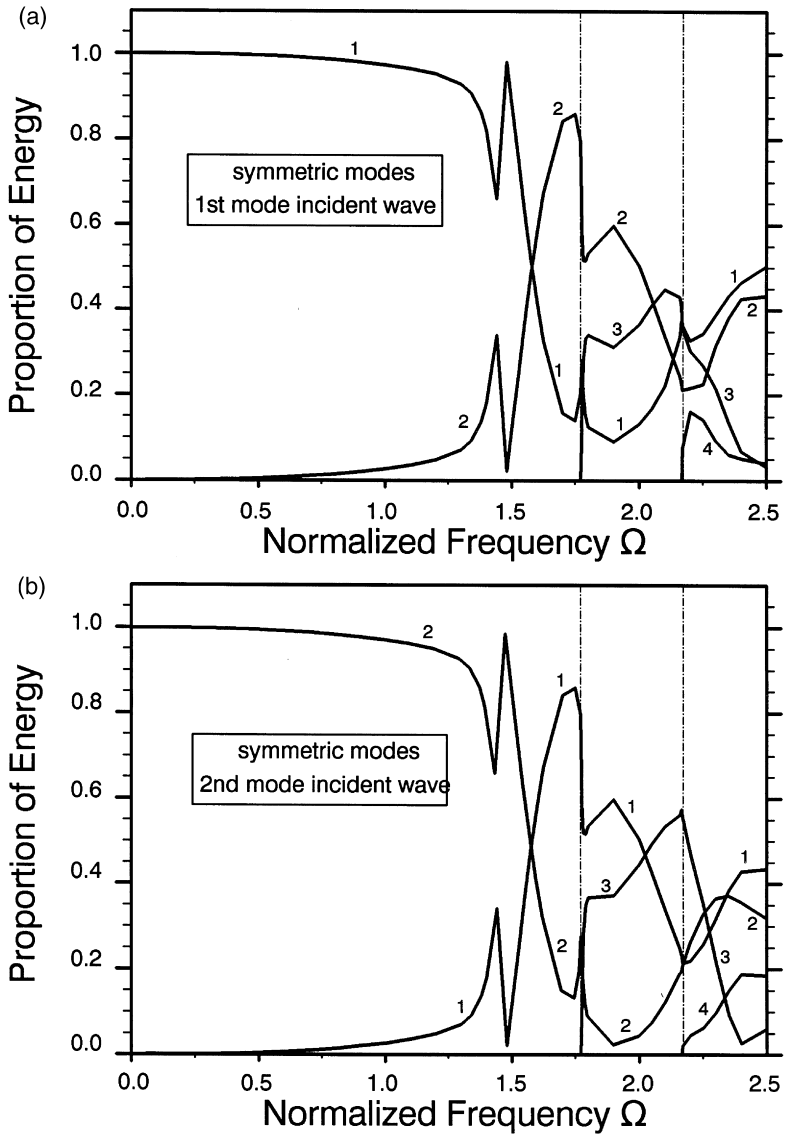

Fig. 9. Energy distributions of the symmetric motions in a three-layer [+30/−30/+30] composite material cylinder.

the reflected motion. The reflected energy distributions for the normalized frequency range ($0 \leq \Omega \leq 2.25$) are shown in Fig. 10a (first mode as incident wave) and Fig. 10b (second mode). The reciprocal nature of the reflected energies of these two modes below the frequency where the third mode cuts on, i.e., that marked by broken vertical line $\Omega \approx 1.76$, at is again evinced as seen from these figures.

7.4. Two layer $\pm 30^{\circ}$ fiber composite rectangular bar

For a two layer rectangular bar with overall height-to-width ratio $H/W = 1/2$, the horizontal mid-

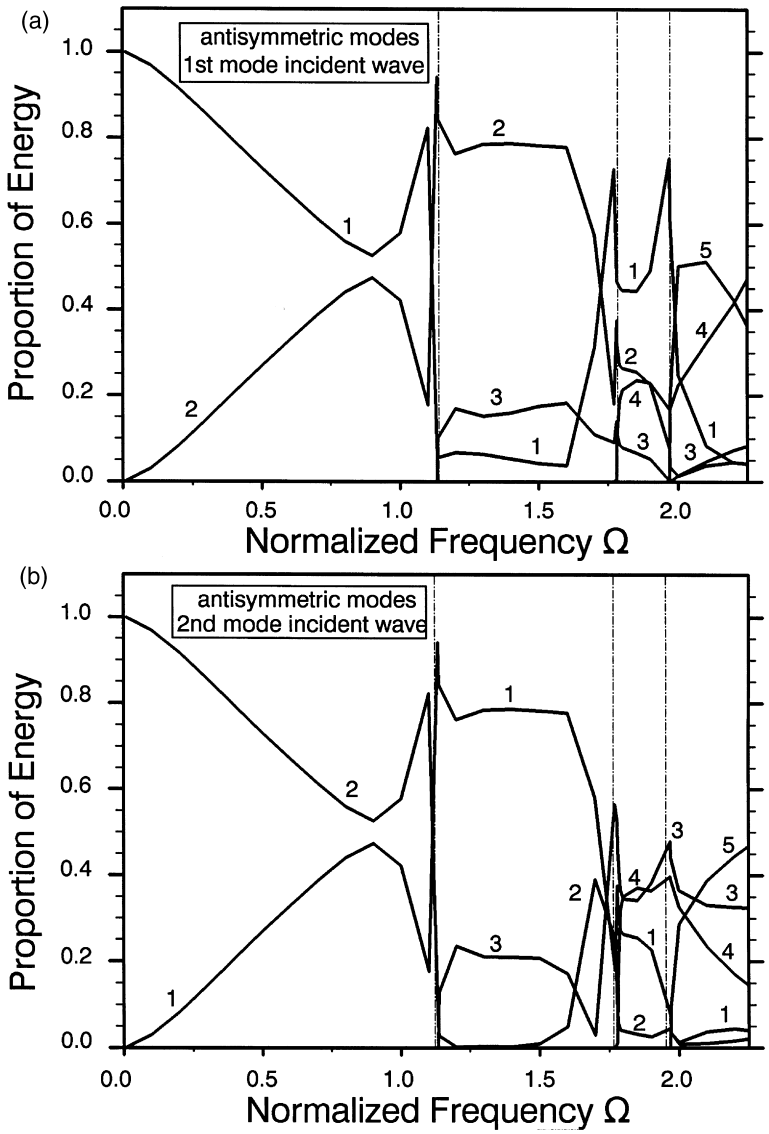

Fig. 10. Energy distributions of the antisymmetric motions in a three-layer [+30/−30/+30] composite material cylinder.

plane of the cross-section is an antisymmetry plane. This cross-section may also be considered to be symmetric with respect to a π-rotation about the propagation axis (i.e., z-axis) through the centroid. The mechanical properties of this cross-section are the same as those of the three layer beam, i.e., those given by eqn (61). There exist two classes of motions in this cross-section, which may be regarded as generalized rotationally symmetric and antisymmetric with respect to the π-rotation about the z-axis. However, unlike the previous three layer cross-section, it does not appear possible to separate these two behavioral classes with a model of one-half of the cross-section with appropriate interface conditions along the entire horizontal mid-plane. Therefore, the entire cross-section was subdivided as shown in

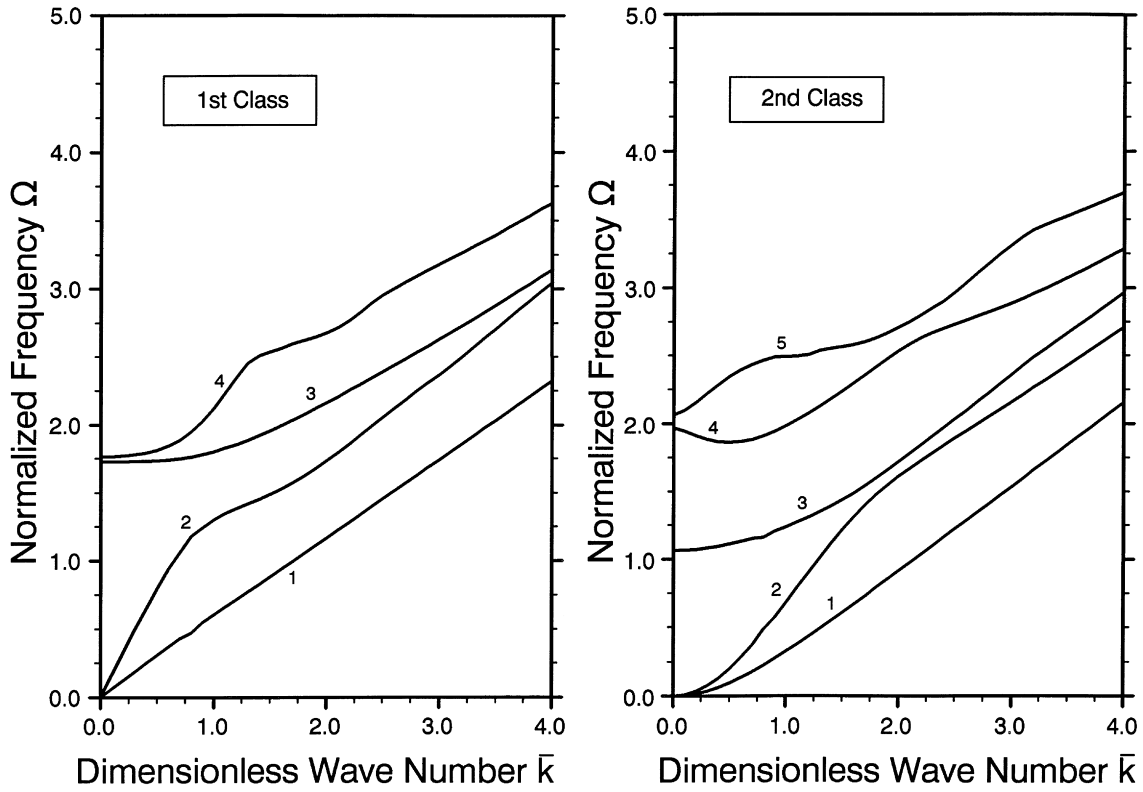

Fig. 11. Frequency spectra for two-layer [+30/−30] composite material cylinder.

Fig. 2. It is noted that any incident wave belonging to one class will not excite reflected motions of the other class.

Frequency spectra for the lowest subset of propagating modes for these two classes of motions are shown in Fig. 11. From the modal patterns of the lowest two modes for long wavelengths (i.e., small normalized wave numbers) of the first class (not presented here for brevity sake), it was observed that they bear strong resemblance to extensional and torsional waves except that they are coupled in both modes. However, strictly speaking they are not extensional nor torsional because their motions are not completely symmetric or antisymmetric about the two cross-sectional coordinate planes. Similar remarks can be made of the lowest two modes of the second class in that they appear to be coupled flexural motions about two axes. However, for this cross-section, these two axes are not orthogonal to each other; one is the x-axis and the other makes an angle of approximately 27° with the y-axis.

For the first class motions, the reflected energy distribution for normalized frequency range ($0 \leq \Omega \leq 2.1$) due to the lowest mode as the incident wave is shown in Fig. 12a, and that with the second wave as incident wave is shown in Fig. 12b. Analogues results for the second class motions over the same frequency range are shown in Fig. 13a and 13b. For both classes, one hundred fifty to two hundred end modes were used depending on the frequency. The reciprocal nature of the energy distributions at frequencies below the third lowest cut on frequency is again observed here for both classes of motions, i.e., at frequencies of $\Omega \approx 1.72$ and $\Omega \approx 1.07$, respectively, for the first and second

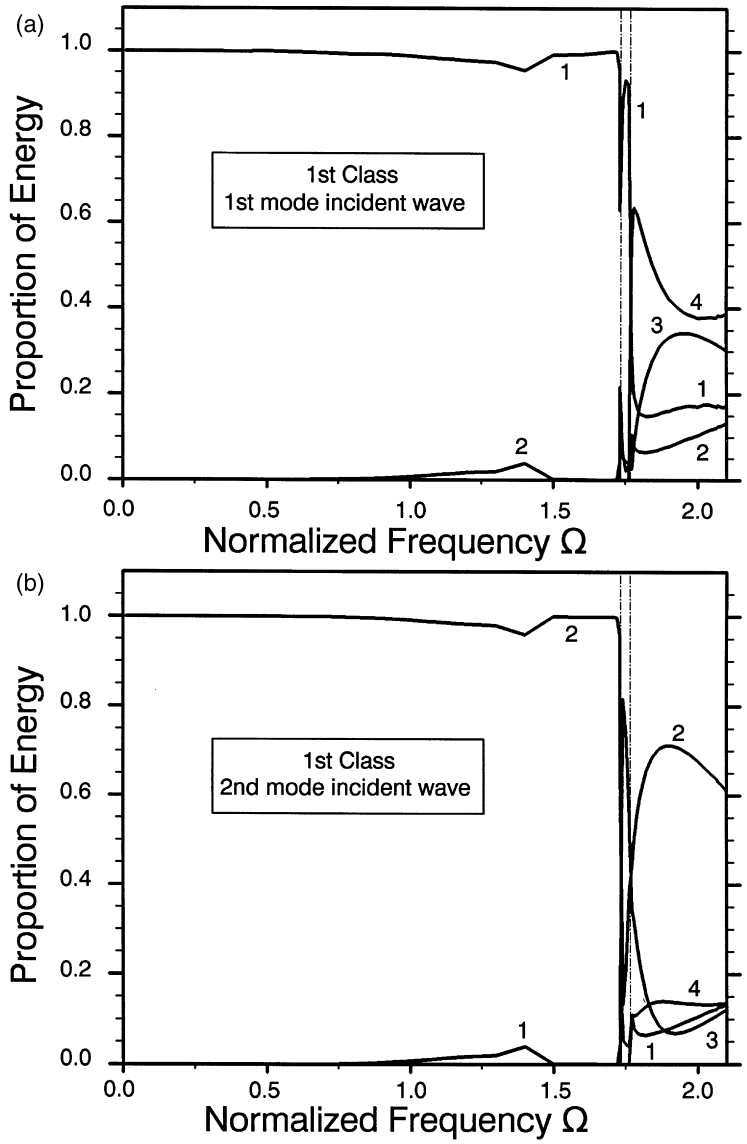

Fig. 12. Energy distributions of first class motions in a two-layer [+30/−30] composite material cylinder.

classes. For frequencies above the third mode, there is considerable distinction in the reflected energies with respect to which mode is taken as the incident wave.

8. Concluding remarks

The reflected motion due to a monochromatic incident wave striking a traction-free end of a cylinder with an arbitrary cross-section was represented by a composition of traveling waves and end modes. These modal data come from two eigenanalyses. The reflection analysis procedure satisfies traction-free

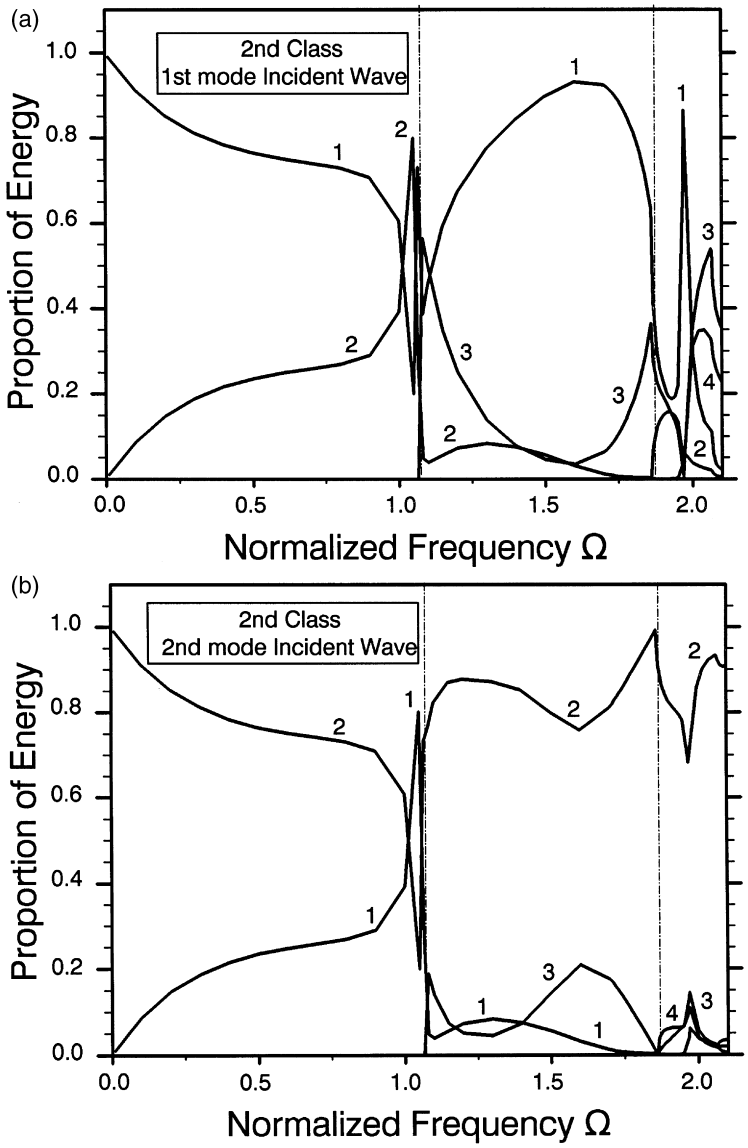

Fig. 13. Energy distributions of second class motions in a three-layer [+30/−30] composite material cylinder.

ends and partitions the incident wave energy into the various reflected traveling waves. The four cross-sections that were considered show the complicated nature in the energy distribution of the reflected waves. To gain physical insight into the frequency dependent phenomena, a detailed study of all the displacement and stress modal patterns must be undertaken.

It is mentioned that the reflection analysis did not considered mathematical singularities that are present due to dissimilar materials at common interfaces. These singularities are generally weaker than those of cracks. They will affect the near field behavior at the free end of the cylinder and will alter the energy distribution in the reflected waves as well as the participation of the various end modes.

Determining the quantitative nature of such singularities would be a worthwhile continuation of this study, which should lead to a more complete understanding of the wave reflection phenomena.

References

Aalami, B., 1973. Wave in prismatic guides of arbitrary cross-section. Journal of Applied Mechanics, ASME 40, 1067–1072.

Bancroft, D., 1941. The velocity of longitudinal waves in cylindrical bars. Physical Review 59, 588–593.

Chree, C., 1889. The equations of an isotropic elastic solid in polar and cylindrical coordinates, their solutions and applications. Transactions of the Cambridge Philosophical Society 14, 250–369.

Davies, R.M., 1948. A critical study of the Hopkinson pressure bar. Philosophical Transactions, Royal Society A240, 375–457.

Dong, S.B., Kazic M., 1989. End modes and their application to wave reflection analysis. Vibration Analysis—Techniques and Applications, DE-Vol. 18–4, 12th Biennial Conference on Mechanical Vibration and Noise. Montreal, Quebec, Canada, pp. 199–208.

Fraser, W.B., 1969. Stress wave propagation in rectangular bars. International Journal of Solids and Structures 5, 379–397.

Gregory, R.D., Gladwell, I., 1989. Axisymmetric waves in a semi-infinite elastic rod. Quarterly Journal of Mechanics and Applied Mathematics 42, 327–337.

Hudson, G.E., 1943. Dispersion of elastic waves in solid circular cylinders. Physical Review 63, 46–51.

Kantorovich, L.V., Krylov, V., 1958. Approximate Analysis for Higher Analysis. Noordhoff, Groningen, Netherlands.

Kynch, G.J., 1957. The fundamental modes of vibration of uniform beams from medium wavelengths. British Journal of Applied Physics 8, 64–73.

Lamb, H., 1917. On waves in an elastic plate. Proceedings of the Royal Society of London A93, 114–128.

Mindlin, R.D., 1959. Waves and vibrations in isotropic, elastic plates. In: Goodier, J.N., Hoff, N.J. (Eds.), Mechanics—Proceedings of the First Symposium on Naval Structural Mechanics. Pergamon Press, Oxford, pp. 199–232.

Nigro, N.J., 1966. Steady-state wave propagation in infinite bars of noncircular cross-section. Journal of the Acoustical Society of America 40, 1501–1508.

Onoe, M., McNiven, H.D., Mindlin, R.D., 1962. Dispersion of axially symmetric waves in elastic rods. Journal of Applied Mechanics, ASME 29, 729–734.

Pao, Y.H., 1962. The dispersion of flexural waves in an elastic circular cylinder—Part 2. Journal of Applied Mechanics, ASME 29, 61–64.

Pao, Y.H., Mindlin, R.D., 1960. Dispersion of flexural waves in an elastic circular cylinder. Journal of Applied Mechanics, ASME 27, 513–520.

Pochhammer, L., 1876. Über die Fortpflanzungsgeschwindigkeiten kleiner Schwingenungen in einem unbegrenzten isotropen Kreiszylinder. Zeitschrift für reine und angewandte Matematik 81, 325–336.

Rattanawangchareon, N., Shah, A.H., Datta, S.K., 1994. Reflection of waves at the free edge of a laminated circular cylinder. Journal of Applied Mechanics, ASME 61, 323–329.

Rayleigh, J.W.S., 1888. On the free vibration of an infinite plate of homogeneous Isotropic elastic matter. Proceedings of the London Mathematical Society 20, 225–234.

Redwood, M., 1960. Mechanical Waveguides. Pergamon Press, Oxford.

Wu, C.H., Plunkett, R., 1967. On the solutions of plates, strips, rods, and cylinders subjected to arbitrary dynamics edge load. SIAM Journal of Applied Mathematics 15, 107–119.